# BEST AVAILABLE IMAGES

Defective images within this document are accurate representations of the original documents submitted by the applicant.

Defects in the images may include (but are not limited to):

- BLACK BORDERS
- TEXT CUT OFF AT TOP, BOTTOM OR SIDES
- FADED TEXT
- ILLEGIBLE TEXT
- SKEWED/SLANTED IMAGES
- COLORED PHOTOS
- BLACK OR VERY BLACK AND WHITE DARK PHOTOS
- GRAY SCALE DOCUMENTS

## IMAGES ARE BEST AVAILABLE COPY.

**As rescanning documents *will not* correct images, please do not report the images to the Image Problem Mailbox.**

(125)

(12) INTERNATIONAL APPLICATION PUBLISHED UNDER THE PATENT COOPERATION TREATY (PCT)

(19) World Intellectual Property Organization
International Bureau

(43) International Publication Date
26 July 2001 (26.07.2001)

PCT

(10) International Publication Number
WO 01/53199 A2

(51) International Patent Classification[7]: C01B 31/00

(21) International Application Number: PCT/US01/01698

(22) International Filing Date: 17 January 2001 (17.01.2001)

(25) Filing Language: English

(26) Publication Language: English

(30) Priority Data:
60/177,075 19 January 2000 (19.01.2000) US

(71) Applicant *(for all designated States except US)*: **MID-WEST RESEARCH INSTITUTE** [US/US]; 425 Volker Boulevard, Kansas City, MO 64110 (US).

(72) Inventors; and
(75) Inventors/Applicants *(for US only)*: **DILLON, Anne, C.** [US/US]; 175 S. 33rd Street, Boulder, CO 80303 (US). **GENNETT, Thomas** [US/US]; 296 Thornell Road, Pittsford, NY 14534 (US). **HEBEN, Michael, J.** [US/US]; 1036 Marion Street, Denver, CO 80218 (US).

(74) Agent: **WHITE, Paul, J.**; National Renewable Energy Laboratory, 1617 Cole Boulevard, Golden, CO 80401 (US).

(81) Designated States *(national)*: AE, AG, AL, AM, AT, AU, AZ, BA, BB, BG, BR, BY, BZ, CA, CH, CN, CR, CU, CZ, DE, DK, DM, DZ, EE, ES, FI, GB, GD, GE, GH, GM, HR, HU, ID, IL, IN, IS, JP, KE, KG, KP, KR, KZ, LC, LK, LR, LS, LT, LU, LV, MA, MD, MG, MK, MN, MW, MX, MZ, NO, NZ, PL, PT, RO, RU, SD, SE, SG, SI, SK, SL, TJ, TM, TR, TT, TZ, UA, UG, US, UZ, VN, YU, ZA, ZW.

(84) Designated States *(regional)*: ARIPO patent (GH, GM, KE, LS, MW, MZ, SD, SL, SZ, TZ, UG, ZW), Eurasian patent (AM, AZ, BY, KG, KZ, MD, RU, TJ, TM), European patent (AT, BE, CH, CY, DE, DK, ES, FI, FR, GB, GR, IE, IT, LU, MC, NL, PT, SE, TR), OAPI patent (BF, BJ, CF, CG, CI, CM, GA, GN, GW, ML, MR, NE, SN, TD, TG).

**Published:**
— *without international search report and to be republished upon receipt of that report*

*For two-letter codes and other abbreviations, refer to the "Guidance Notes on Codes and Abbreviations" appearing at the beginning of each regular issue of the PCT Gazette.*

(54) Title: SINGLE-WALL CARBON NANOTUBES FOR HYDROGEN STORAGE OR SUPERBUNDLE FORMATION

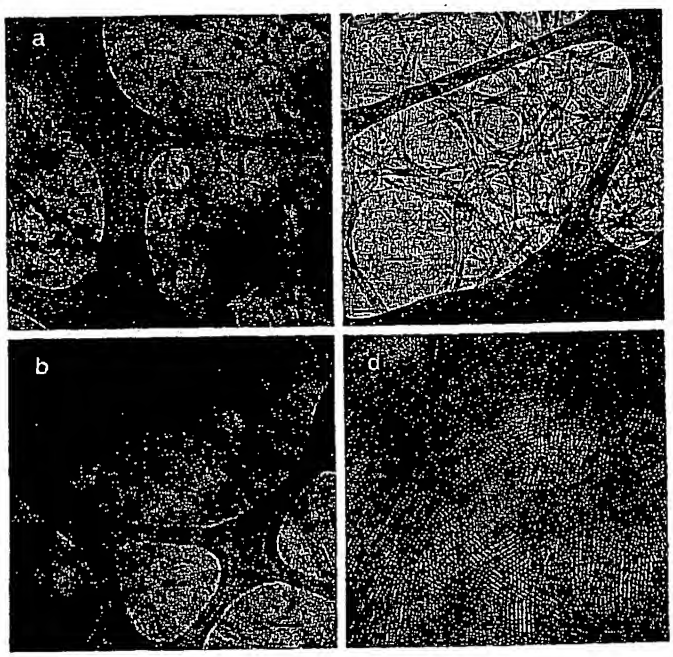


(57) Abstract: A method of processing single-walled carbon nanotubes (SWNTs) in the formation of superbundles or for use in hydrogen storage, or both, is provided comprising the steps of mixing a SWNT substrate in a solvent solution into a suspension, and agitating the suspension using an ultrasonic energy means.

WO 01/53199 A2

purified bundles 5-10 nm in width.

p.11 bundles - 0.4-1 micron in diameter 5-10 microns in length

cut 1-5 microns in length

Aspect ratio 1000:1

# Single-Wall Carbon Nanotubes For Hydrogen Storage Or Superbundle Formation

## Technical Field

This invention relates to single-wall carbon nanotubes ("SWNTs"), and in particular to a method of processing SWNTs for use in hydrogen absorption or superbundle formation.

## Background Art

As is well known in the materials science art, there has been interest in the mechanical, electrical, physical, and optical properties of SWNTs. This interest is not surprising when considering the broad impact that these materials will make in the areas of science and technology, whether as applied in the form of super-strong composites, nanoelectronics, or to the safe storage of hydrogen which is vital in the development of hydrogen fuel cells or combustion engines. Indeed, the shape of SWNTs suggests that these composite materials would serve as an ideal hydrogen storage container.

In order to further these applications, one must evaluate the intrinsic mechanical and electrical properties of SWNTs. A distinct disadvantage of the prior art has heretofore been the inability in evaluating these properties when using the current synthesis and purification procedures, which result in SWNTs having a random orientation, diameter, and length distribution. Moreover, many electrical and mechanical applications further require an orderly cutting or alignment of the individual nanotubes which comprise SWNT composite materials. For hydrogen storage, one must further resolve the problem of processing SWNTs, to either open, reorganize, cut, or functionalize them, without consuming the nanotubes in the process.

The ability to form organized SWNT superbundles is also important because of the possibility of performing macroscopic analyses on well-defined samples. Of particular interest would be polarized Raman spectroscopy studies that would allow unambiguous assignment of observed spectral bands to specific types of SWNTs. Superbundle formation may also be a first step towards the production of longer. Control over the superbundle length and diameter at either the formation step or subsequently through the use of other

means may provide a route to electrical connectors, or perhaps superbundle crystals and films that would be useful as hydrogen adsorbents or gas transport membranes.

It is also desirable in some applications to obtain high levels of hydrogen storage in SWNT materials at ambient conditions in a matter of minutes or seconds. In 1997 single-walled carbon nanotubes were first shown to adsorb hydrogen at near ambient temperature and pressure following heating in vacuum to 973K(1). It was subsequently reported that graphite nanofibers could adsorb up to 67 wt% hydrogen at room temperature and 120 atm(2), however, these results could not be corroborated(3). Hydrogen adsorption on purified, cut SWNTs was then shown to exceed 8 wt% at ~160 atm and 80 K(4). Lithium doped carbon nanotubes were shown to adsorb hydrogen at ambient pressure to ~20 wt% between 473-673 K while potassium doped samples adsorbed ~14 wt% at room temperature. However, the potassium doped nanotubes were found to be oxidized rapidly upon exposure to air(5). Recently, acid treated large diameter (1.85 nm) SWNTs were shown to adsorb 4.2 wt% hydrogen at room temperature and about 100 atm. The samples could be charged to 70% of the whole adsorption capacity in ~ 1 hr (6).

**Disclosure of Invention**

The present invention is intended to provide a method for processing SWNTs for use in high density hydrogen storage or in electrical or mechanical applications.

It is further intended that the present invention provide a process of realignment and collapse of the small SWNT bundles into much larger superbundle configurations.

It is further intended that the present invention provide a process of forming SWNT materials which are capable of at least 6-7 wt% hydrogen adsorption at ambient conditions.

Additional advantages of the present invention will be set forth in part in the description that follows and in part will be obvious for that description or can be learned from practice of the invention. The advantages of the invention can be realized and obtained by the method particularly pointed out in the appended claims.

Briefly, the invention provides a method of processing single-walled carbon nanotubes (SWNTs) in the formation of superbundles or for use in hydrogen storage, or both, comprising the steps of mixing a SWNT substrate in a solvent solution into a suspension, and agitating the suspension using an ultrasonic energy means.

**Brief Description of Drawings**

Figure 1a is a transmission electron microscope image of crude 4.2 W laser generated SWNT soot.

Figure 1b is a transmission electron microscope image of a crude material which was refluxed for 16 h in 3M $HNO_3$.

Figure 1c is a transmission electron microscope image of purified SWNTs produced by oxidizing the acid treated sample for 30 min. in air at 550 °C.

Figure 1d is a transmission electron microscope image of purified tubes at high magnification after annealing to 1500 °C in vacuum.

Figure 2a is a thermal gravimetric analysis of 1-2 mg samples ramped from 25 - 875 °C at 5 degrees per minute in a platinum sample pan under 100 sccm flowing air. The figure shows materials produced at a laser power of 4.2 W; fully purified, crude soot, and crude soot after a 16 h reflux in 3M $HNO_3$. The data for the refluxed material was normalized to 100 wt % at 100 °C to compare dry weights.

Figure 2b is a thermal gravimetric analysis of 1-2 mg samples ramped from 25 - 875 °C at 5 degrees per minute in a platinum sample pan under 100 sccm flowing air. The figure shows materials produced with 6W of laser power. Samples were refluxed in 3M $HNO_3$ for 4, 16, and 48 h. These curves were normalized to 100 wt % at 100 °C to compare dry weights, and then re-normalized to account for the different weight losses in the $HNO_3$ refluxes.

Figure 3 is a Raman spectra obtained at 488 nm with a resolution of 2-6 $cm^{-1}$ for purified, crude, and crude material which was refluxed for 16 h in 3M $HNO_3$ acid. The inset of the figure shows the region from 1200 - 1500 $cm^{-1}$ at an amplified intensity scale.

Figure 4a is a is a transmission electron microscope image of purified tubes at high magnification.

Figure 4b is a is a transmission electron microscope image of purified tubes formed into "superbundles" of 0.5 to 2 microns in width.

Figure 4c is a transmission electron microscopy image of a superbundle from figure 4b at higher magnification.

Figure 5a is a transmission electron microscope image of SWNT superbundles extracted from water at low magnification illustrating the length of the fiber.

Figure 5b is a transmission electron microscope image of SWNT superbundles extracted from water at high magnification illustrating the width and dense packing of the superbundle.

Figure 6 is a transmission electron microscope image of purified SWNTs following ultrasonication in 5M $HNO_3$. The apparently endless ropes seen after purification have been "cut" into compact bundles ~ 1 - 5 microns in length.

Figure 7 shows temperature programmed desorption spectroscopy data from both SWNTs and microcrystalline graphite after a 10 min. hydrogen exposure at 500 torr. Both samples had been sonicated in dilute $HNO_3$ for 16 hours.

Figure 8a displays the hydrogen desorption signal from a $HNO_3$ sonicated SWNT sample following a 500 torr hydrogen exposure at room temperature. The sample remained at room temperature while the vessel was evacuated.

Figure 8b displays the $CO_2$ TPD signal after a hydrogen dose as in Figure 8a was followed by a 10 min. $CO_2$ dose at 500 torr.

Figure 8c displays the TPD signal for the hydrogen which also evolved along with the $CO_2$ shown in Figure 8b.

Figure 9a is a Raman spectrum from purified SWNTs.

Figure 9b is a Raman spectrum obtained after purified SWNTs had been sonicated at 90 $W/cm^2$ for 4 hours in 5M $HNO_3$.

Figure 9c is a Raman spectrum obtained after purified SWNTs were sonicated at 90 $W/cm^2$ in 5M $HNO_3$ for 4 hours and then degassed in vacuum to 973 K.

Figure 9d is a Raman spectrum obtained after purified SWNTs were sonicated at 90 $W/cm^2$ in 5M $HNO_3$ for 4 hours, degassed in vacuum to 973 K, and then exposed to hydrogen at 500 torr.

Figure 9e is a Raman spectrum obtained after purified SWNTs were sonicated at 90 $W/cm^2$ in 5M $HNO_3$ for 4 hours, degassed in vacuum to 973 K, exposed to hydrogen at 500 torr, and then heated again to 973 K in vacuum.

## Best Mode for Carrying Out the Invention

Unless specifically defined otherwise, all technical or scientific terms used herein have the same meaning as commonly understood by one of ordinary skill in the art to which this invention belongs. Although any methods and materials similar or equivalent to those described herein can be used in the practice or testing of the present invention, the preferred methods and materials are now described.

**Example 1**

Referring now to the drawing figures, SWNT materials were synthesized by a laser vaporization method. A single Nd:YAG laser was used which produced gated laser light ranging in duration from 300 to 500 ns. The gated laser light contained numerous short laser pulses ranging in duration from 5 to 15 ns. The emission wavelength was 1064 nm and at an average power of 4 - 8 W. Material was produced at rates of 75 - 150 mg / h. Targets were made by pressing powdered graphite doped with 0.6 at % each of Co and Ni in a 1 1/8 inch dye. Crude soot containing SWNTs was produced at 800 - 1300 °C, with 500 Torr Ar flowing at 100 sccm. The transmission electron microscope ("TEM") image in Figure 1a reveals the components of the laser-generated material. Bundles of SWNTs span between large agglomerations of amorphous and micro-crystalline carbon which contain metal nanoparticles. Typical raw materials were estimated to contain ~ 20 - 30 wt % SWNTs by a detailed analysis of numerous different TEM images, A.C. Dillon, P.A. Parilla, K.M. Jones, G. Riker & M.J. Heben, *Mater. Res. Soc. Conf Proc.* 1998, *526, 403*. Inductively coupled plasma spectroscopy ("ICPS") indicated the laser-generated crude material has the same metal content as the targets (~ 6 wt %).

Approximately 80 mg of crude soot produced at 4.2 W was refluxed in 60 ml 3M $HNO_3$ for 16 h at 120 °C. The solids were collected on a filter that allows ready separation of the nanotubes, such as 0.2 μm polytetrafluoroethylene coated polypropylene, and rinsed with deionized water. After drying, an 82 wt % yield was obtained. The weight lost is consistent with the digestion of the metal and an additional ~ 12 wt % of the crude material. The reflux caused the non-nanotube carbon fractions to be redistributed as a uniform coating on the SWNTs as seen in Figure 1b. The material was then oxidized in stagnant air inside a

tube furnace at 550 °C for 30 minutes. In this manner, the carbon coating was completely removed leaving behind pure SWNTs, corresponding to ~ 20 wt % of the crude material (Figure 1c). Figure 1d displays the purified tubes at high magnification. Thermal gravimetric analysis ("TGA") revealed the purity of the isolated SWNTs. The decomposition temperature (Td) is 735 °C, as determined by the derivative of the TGA curve, for the pure SWNTs displayed in Figure 2a. The purified tubes are very stable presumably due to the lack of dangling bonds or defects at which oxidation reactions may initiate. The final purity is estimated to be >98 wt % since <1 wt % is consumed below 550 °C, and <1 wt % remains above 850 °C. The metal content of these pure SWNTs was measured to be below 0.5 wt % by ICPS.

TGA was also used to evaluate the crude and acid-refluxed materials to illuminate the key features of the purification process. The data for the crude soot (Figure 2a) shows a slight increase in weight at low temperatures due to the oxidation of the Ni and Co metals. The carbonaceous fractions begin to combust at ~370 °C and are mostly removed by oxidation below 600 °C. A small final weight loss at ~650 °C can be attributed to oxidation of surviving SWNTs (~4 wt %). The majority of SWNTs in the crude soot are combusted along with the other carbonaceous materials at lower temperatures. The weight remaining at 875 °C corresponds to the weight expected for the oxidized metals (~ 8 wt %).

The TGA data is different after crude materials are refluxed for 16 h in 3M $HNO_3$ (Figure 2a). A first thing to note is that refluxed samples getter as much as 10 wt % water from lab air, while purified and crude samples remain relatively dry. More importantly, the onset of non-nanotube decomposition occurs at a lower temperature for the refluxed material and is completed before the onset of SWNT combustion. A plateau extending from 550 to 650 °C is clearly evident in the TGA data because the oxidation now occurs in two separate regimes. The sample weight is reduced to approximately zero by 850 °C since all carbonaceous materials have been removed and essentially no metal is left. The acid treatment not only removes the metal but also produces carboxyl, aldehyde, and other oxygen - containing functional groups on the surfaces of the non-nanotube carbonaceous

fractions. As a result, the coating is extremely hygroscopic and reactive towards oxidation, enabling efficient purification.

The combustion of non-nanotube fractions is essentially complete at the inflection point in the TGA curve of the refluxed soot at 560 °C. At this point, the sample consists of only pure SWNTs which amount to ~26 wt % of the dry refluxed material, or ~21 wt % of the pre-reflux weight. This latter value is in excellent agreement with the yield after refluxed material was heated to 550 °C in stagnant air (~20 wt %), and considerably higher than the tube content determined by TGA analysis of the crude material (~4 wt %). The quantitative agreement between the bulk oxidation in stagnant air and the TGA measurements under dynamic conditions suggests that neither route consumes an appreciable amount of SWNTs. In fact, neither longer times in stagnant air at 550 °C (up to 1 h) nor holding at 550 °C during TGA experiments produces further significant weight loss. The final product is pure since the weight-loss proceeds as expected for oxidation of a single phase above 550 °C, and the TEM image of Figure 1c shows only SWNTs.

To determine if tubes are damaged or consumed during the dilute acid reflux, TGA was performed on materials which were refluxed for 4, 16, and 48 h in 3M $HNO_3$ (Figure 2b). Materials for these experiments were produced with 6 W of laser power. The TGA data was adjusted for the dry-weight lost during reflux so that the y-axis represents the wt % remaining of the initial crude material. The data for the 4 and 16 h refluxes completely overlay at temperatures above ~450 °C, and a plateau associated with SWNT stability is observed at 540 °C and a SWNT content of 17 wt %. The data sets are virtually identical at the higher temperatures despite the difference in the material weights which were lost during the refluxes. Since the SWNT content is determined to be the same in both cases, neither reflux consumes a significant number of tubes. As discussed earlier, tubes are not consumed by oxidation below 550 °C, so the 17 wt % value can be taken as an accurate assessment of the SWNT content in the crude soot. Once again, this value was found to be in good agreement with the yield determined by batch oxidation at 550 °C of material refluxed for 16 h in 3M $HNO_3$. It is interesting to note that the SWNT content in the 6 W material is

lower than in the 4.2 W material. Such a quantitative comparison was not possible prior to the purification and assessment methods disclosed herein.

Unlike the 16 h process, the 4 h reflux did not always permit good purification by oxidation. In these cases, a TGA curve very similar to that of the crude material was observed. The oxidation reactions are no longer well-separated after a 48 h reflux (Figure 2b), and there is only a slight indication of a SWNT stability plateau at ~ 625 °C. The affinity for water is considerably less than in either the 4 or 16 h samples. The thick, uniform, hydrophilic carbon coating produced after 16 h of refluxing and thought to be necessary for purification was not observed by TEM. Instead, a generally thinner and patchy film was found along with occasional agglomerations. In contrast to the TEM data of Figure 1b, SWNTs could be readily imaged and portions of tubes were observed to be sharply angled, cut and damaged. The extended reflux digests most of the non-nanotube carbon and begins to attack the SWNTs. These cut and defective tubes are more susceptible towards oxidation such that only ~8 wt %, or < 50 % of the tubes known to be present, are found at the inflection point in the curve at 625 °C (Figure 2b).

Raman spectroscopy further elucidates the $HNO_3$ reflux process. The Raman spectra displayed in Figure 3 for purified and crude materials both exhibit a strong feature at 1593 $cm^{-1}$ with shoulders at 1567 and 1609 $cm^{-1}$ as expected for the SWNT tangential C-atom displacement modes. However, the broadened feature at 1349 $cm^{-1}$ in the crude spectrum indicates the presence of impurities and a contribution from the disordered $sp^2$ carbon "D band" of non-nanotube graphite components, P.C. Eklund, J.M. Holden & R.A. Jishi, *Carbon* 1995, 33,959; Y. Wang, D.C. Alsmeyer & R.L., McCreedy, *Chem. Mater.* 1990, 2, 557. Unlike other reports, G. Rinzler, *et al., Applied Physics A* 1998, *67*, 29; S. Bandow, *et al., J. Phys. Chem. B* 1997, 101, 8839, no spectral evidence for $C_{60}$ was ever detected in any of our materials. After the 16 h reflux, the D band intensity is significantly increased indicating decreasing domain size (Figure 3). Also, a signal derived from the fundamental $E_{2g}$ mode of disordered graphite is observed where the SWNT modes are expected. The disordered graphite coating (Figure 1b) evidently prohibits observation of the resonantly enhanced SWNT modes. This is striking since the SWNT content in the 16 h $HNO_3$ treated

sample is actually higher than in the crude material, and demonstrates that Raman spectroscopy can be poorly suited for determining SWNT contents in certain types of samples. The D-band is narrower in purified materials as observed by others (S. Bandow, A.M. Rao, D.A. Williams, A. Thess, R.E. Smalley, P.C. Eklund, J. Phys, Chem. B. 1997, 101 (8839-8842) presumably due to curvature-induced enhancement of electron-phonon coupling (J. Kastner, T. Pichler, H. Kuzmany, S. Curran, W. Blau, D.N. Weldon, M. Delamesiere, S. Draper, H. Zandbergen, Chem. Phys. Lett. 1994, 221, 53-58).

Conclusively, the 16 h 3M $HNO_3$ reflux decreases the domain size of the disordered carbon and produces a uniform carbon coating on the SWNTs without damaging them. Our own temperature programmed desorption studies show that the nitric acid reflux introduces reactive functional groups onto the surfaces of the non-nanotube carbon material. These two effects serve to maximize the surface area of the nonnanotube carbon and provide for enhanced oxidation kinetics. Furthermore, since the functionalized coating is oxidized at lower temperatures, and the coating is evenly distributed, the heat generated by the exothermic reactions does not initiate oxidation of SWNTs. In contrast, SWNTs in raw materials are consumed simultaneously with impurities because the oxidation of agglomerated impurities generates local "hot spots". It is a combination of the high-surface-area, decreased domain size, degree of functionalization, and uniformity of the carbon film produced by the 16 h 3M $HNO_3$ reflux that allows non-destructive purification of SWNTs with air oxidation.

The purified SWNT soots were mixed in a aqueous 5M $HNO_3$ solution. Using an ultrasonic probe, a concentrated ultrasonic energy was directed into the solution. The resultant cavitation produced microscopic domains of extremely high temperature. The combination of the ultra sonic energy, high temperatures, and oxidative strength of the $HNO_3$ solvent provided a reproducible cut and an increase in bundle size or both of the SWNTs. A hydrogen adsorption analysis for the SWNTs cut using the 5M $HNO_3$ solution demonstrated an extremely high SWNT hydrogen affinity, in the range of 7 % w/w. The purified bundles, used as the starting material and shown in Figure 4a, were 5 to 10 nm in width.

Example 2

A single Nd:YAG laser(1064 nm) was employed to synthesize the carbon nanotubes from 1.2 at % metal doped (50:50 Co/Ni) pressed graphite targets. The targets were placed in a quartz tube that was heated to a temperature of 1200 °C in a clam-shell furnace. With the laser operating at a frequency of 10 Hz, the laser power and beam size were adjusted to provide ~20 J/pulse-cm$^2$ at a ~450 ns pulse width. An argon flow of 100 sccm at 500 torr was maintained through the reaction vessel for the duration of the synthesis. The raw soot was purified by refluxing in 3M nitric acid for 16 hr, filtering and washing with dionized water on a polytetraflouroethylene (PTFE) filter, and then heating the obtained paper in air for 30 min at 550 °C. This procedure results in tubes of greater than 98 wt.% purity when target material is not sputtered and trapped in vaporized soot. A representative TEM image of the resultant pure tubes is shown in Figure 4a. The random orientation and small size of the long bundles are apparent.

The SWNTs exist as a random tangle because of the conditions under which they are synthesized and purified. The tubes are formed within the high temperature plasma generated by the laser striking the graphite target, and their formation is rapidly quenched as the tubes diffuse out of the plasma plume. The resulting SWNTs exist in small bundles and are accompanied by other graphitic and amorphous carbon fractions as well as metal nanoparticles. The purification process succeeds in removing the non-nanotube carbon fractions and the metals. However, the purification process still results in a random orientation of tube bundles which have ~ 5 - 20 nm diameters.

A 1.0 mg sample of purified SWNTs was placed in a cylinder containing 10 ml of deionized water or other polar hydrophilic solvents or solvent mixtures. A Heat Systems-Ultrasonics Inc. model w-220F Cell Disrupter was submersed into the solution and the power was slowly increased to 90 watts/cm$^2$. The ultrasonic agitation was continued for a maximum of 120 minutes. Normally, SWNTs are not dissociated in aqueous solution without the use of surfactants. With the use of the ultrasonic probe, however, the SWNT sample was almost immediately dispersed throughout the solvent. The SWNT material agglomerated in the solution when the ultrasonic agitation was turned off. Gentle shaking of the solution redistributed the tube agglomerations into an apparently homogeneous

suspension. If the sonicated solution was allowed to settle, a thin layer of SWNT superbundles were observed at the solvent interface. At this point the isolation of the superbundles was achieved via several different procedures and on a series of substrates. For example, a TEM grid could be used to lift off the SWNT interface layer to extract fibers. The resulting isolated SWNT superbundles were approximately 0.4 - 1 micron in diameter, 5-10 microns in length, and present in many locations on the TEM grid. Other collection strategies included the use of silver, platinum, silicon or highly ordered pyrolytic graphite substrates, sonication of the tubes in the presence of the substrate, or spin coating the sonicated solution onto a prepared substrate surface. Preliminary results indicate that the polarity of the solvent greatly affects the size and density of the bundles after sonication. Solvents such as toluene, hexane, alcohols and water have been employed so far, and SEM images showed that sonication in toluene produces the smallest bundle diameters (≈50 nm) while water produces the largest (≈1micron).

Figures 4b displays a TEM image of SWNTs on a grid dipped into the film formed following sonication in a 50:50 methanol/water mixture. The large superbundles are readily apparent, and it is clear that some of these superbundles are completely isolated. An image of an isolated bundle at higher magnification is displayed in Fig. 4c. The superbundle configuration probably arises from the minimization of the interactions between hydrophobic SWNT surfaces and the hydrophilic solvent maximizing the vVan der Waals interactions along the axial length of the tubes. The extent of collapse of the superbundle into a tight bundle depends upon solvent composition. Figure 5a displays a TEM image of a more collapsed bundle extracted from water. The dense bundle is displayed at higher resolution in Figure 5b. Some of the bundles extracted from water were so dense that a TEM image could not be obtained as the electron beam could not penetrate through the tight nanotube packing. However, these bundles were also shown to contain aligned tubes using scanning electron microscopy.

**Example 3**

A single Nd:YAG laser (1064 nm) was rastered across 1.2 at % metal doped (50:50 Co/Ni) pressed graphite targets in a quartz tube that was heated to 1200ŝC. The laser was

operated at a frequency of 10 Hz, at ~10-30 J/pulse-cm2 with an ~ 450 ns pulse width. Argon flowing at 100 sccm at 500 torr was maintained through the reaction vessel for the duration of the synthesis. The raw soot was purified by refluxing in 3M nitric acid for 16 hr, filtering and washing with de-ionized water followed by air oxidation for 30 min at 825 K. The $H_2$ adsorption capacity of various SWNT samples were probed by a previously described temperature programmed desorption (TPD) technique. Dillon, A.C. et al., *Nature* 1997, 386, 377. Initially, ~ 0.3 - 1 mg samples were degassed in vacuum up to 823-973 K at1 K/s. Room temperature $H_2$ exposures between 10-500 torr for several seconds were then sufficient to achieve a maximum hydrogen adsorption. Partial hydrogen coverage was obtained following $H_2$ exposure at only 10 mtorr. The sample was generally cooled to 90 K prior to evacuation of the TPD chamber in order to quickly obtain a base pressure of ~5 x $10^{-8}$ torr. The cooling process also ensured that hydrogen which could desorb from the sample near room temperature remained on the sample before acquiring TPD spectra. The hydrogen desorption signals from SWNTs were calibrated using known $H_2$ desorption signals from 0.3 - 1 mg samples of $CaH_2$. The calibration was confirmed by performing thermal gravimetric analyses on a 1mg SWNT sample charged with hydrogen. The hydrogen wt% measured by the two different methods was within 10%.

Previously a degas to 973 K in vacuum was sufficient to activate hydrogen adsorption on arc-generated SWNTs. Dillon, A.C. et al., *Nature* 1997, 386, 377. However in applying the same experimental methods to the very long laser-generated nanotube bundles no significant $H_2$ adsorption was observed for either the crude or purified materials. In order to activate the hydrogen adsorption properties ~ 1-3 mg of the purified laser-generated material was placed in a cylinder containing 20 ml of 5M $HNO_3$. A Heat Systems-Ultrasonics Inc. model w-220F Cell Disrupter ultrasonic probe was then employed to agitate the solution for time periods ranging from 20 minutes to 16 hrs at powers ranging from 25 - 250 W/cm2. The final adsorption capacity of the SWNT samples varied between 2-7 wt% depending on the material, the sonication power, the sonication time and the sample degas temperature. Once the unique hydrogen adsorption properties were obtained, the samples remained activated for at least 8 months. The adsorption was maximized following sonication of purified SWNTs for 24 hrs at 90 W/cm$^2$ with a subsequent degas to 825 K.

Figure 6 displays a typical TEM image of purified SWNTs following ultrasonication in 5M $HNO_3$. Here the as-synthesized seemingly endless ropes of SWNTs have been "cut" into compact bundles ~ 1 - 5 microns in length. The average bundle diameter has also been increased and the tubes have been reorganized and functionalized. Upon degassing the cut SWNT samples in vacuum, NO, $H_2O$, $CO$,$CO_2$, $H_2$ and low molecular weight hydrocarbons are observed. The desorption of NO is consisted with the intercalation of nitric acid in the nanotube bundles. The presence of the other species may be explained by the presence of carboxyl or hydroxyl groups and hydrogen at the nanotube ends or at defects generated by the cutting procedure. Figure 7 displays the $H_2$ TPD spectrum of a degassed SWNT sample following a brief room temperature $H_2$ exposure at 500 torr. The sample was sonicated in dilute $HNO_3$ for 16 hrs and degassed to 825 K resulting in hydrogen adsorption of 6.5 wt%. The spectrum is characterized by two separate desorption signals peaked at 370 and 630 K indicating at least two unique hydrogen adsorption sites. The hydrogen corresponding to the signal peaked at 370 K could be evolved by holding the sample at room temperature overnight in vacuum. Holding the SWNT sample at 423 K for only 8 minutes also resulted in complete evolution from the low temperature site which corresponds to ~2.5 wt%. In order to desorb all of the hydrogen from the higher temperature site it was necessary to heat the sample between 475-850 K. Figure 7 also displays the hydrogen desorption signal from micro crystalline graphite following the same pre-treatment and $H_2$ exposure as the optimized SWNT sample. The graphite sample apparently has two $H_2$ adsorption sites that are very similar to the SWNT sample as there are two desorption peaks at ~380 and 610 K. It is interesting however that the graphite hydrogen adsorption is only ~19 % of the $H_2$ adsorption observed for an SWNT sample of the same mass following the same preparation.

Both of the SWNT hydrogen adsorption sites are effectively "capped" by the adsorption. This phenomena was revealed in an experiment where a standard hydrogen exposure to cut SWNTs was followed by a room temperature 10 min. 500 torr exposure to $CO_2$. The sample was cut for 4 hrs at 90 W/cm$^2$ resulting in a total hydrogen adsorption capacity of ~ 3 wt%. Figure 8 displays the hydrogen desorption signal from the SWNT sample following a 500 torr hydrogen exposure at room temperature without any subsequent

cooling of the sample. The spectrum is very similar to the spectrum observed for the 16 hr cut (Fig. 7) with two peaks at ~ 420 K and 602 K. However, the lower temperature peak is slightly smaller and shifted to a higher temperature due to the absence of cooling while the hydrogen exposure was pumped out of the chamber. Figure 8b and c display TPD desorption signals of $CO_2$ and $H_2$ respectively when an identical hydrogen exposure was followed by a $CO_2$ exposure for 10 min. at 500 torr. The small $CO_2$ desorption signal peaked at 400 K demonstrates the existence of a small population of $CO_2$ adsorption sites on the SWNT sample. Surprisingly, however the $H_2$ desorption signals are both shifted to higher temperature by ~ 50 K. It appears that the hydrogen does not begin to desorb from the SWNTs until a significant portion of the $CO_2$ has already evolved suggesting that the $CO_2$ in fact blocks the hydrogen desorption process. In a subsequent experiment the sample was exposed to $CO_2$ for 10 min at 500 torr at room temperature and then exposed to $H_2$ under the same conditions. Subsequent TPD revealed only a $CO_2$ desorption signal, similar to that seen in Figure 8b with no hydrogen absorption, demonstrating that carbon dioxide completely blocks hydrogen adsorption sites. $CO_2$ also apparently "caps" the SWNTs upon exposure to air. Samples charged with hydrogen and exposed to atmosphere were shown to desorb first $CO_2$ and then $H_2$ several weeks later without a significant loss in the stored hydrogen. This effective "capping" of the SWNTs by $CO_2$ may prove significant to the commercial development of SWNTs for a hydrogen storage system.

Raman spectroscopy was employed to elucidate the mechanism of the unique room temperature hydrogen adsorption on SWNTs. Raman spectra were obtained using a 50 mW Ar ion laser (488 nm) with a resolution of ~ 4-6 $cm^{-1}$. Figure 9 displays a series of Raman spectra between 1500 - 1700 $cm^{-1}$ collected from SWNT samples throughout the pretreatment and $H_2$ adsorption process. The initial spectrum of the purified SWNTs (Fig. 9a) exhibits two strong features at 1597 and 1571 $cm^{-1}$. These features are slightly shifted from their characteristic occurrence at 1593 and 1567 $cm^{-1}$. Figure 9b displays the Raman spectrum of the purified sample following sonication in 5M $HNO_3$ for 4 hr at 90 $W/cm^2$. The two features are now broadened and further shifted to 1599 and 1575 $cm^{-1}$ with their intensity quite dramatically reduced. Following degassing in vacuum to 1000 K however the Raman intensity returns, and the features are shifted back to their characteristic values of

1593 and 1567 $cm^{-1}$ (Fig. 9c). Surprisingly, Figure 93d reveals that subsequent exposure to $H_2$ at 500 torr again results in a loss in Raman intensity and a shift to 1596 and 1570 $cm^{-1}$. The intensity of the Raman signal is again restored by heating in vacuum to 1000K resulting in the evolution of the adsorbed hydrogen (Fig. 9e). A similar somewhat less reversible loss in intensity and slight shifting was observed for features attributed to the radial breathing modes between 162-203 $cm^{-1}$.

The reversible shift to higher frequency in Raman spectral bands observed in Figure 9 is indicative of charge transfer to an acceptor species. The SWNT purification process results in some degree of intercalation and functionalization as indicated by the desorption of NO, $H_2O$, CO, $CO_2$, $H_2$ and hydrocarbons versus heating in vacuum to ~1500 K. The purified sample had been annealed to 825 K in air. This should result in the desorption of the $H_2O$, $CO_2$ and NO species. However, the desorption of chemisorbed hydrogen from purified uncut SWNTs occurs between ~ 900-1500 K. Apparently, the chemisorbed hydrogen is acting as an electron acceptor and produces the shift in the Raman spectrum of the purified SWNTs to 1597$cm^{-1}$. The further shift to 1599 $cm^{-1}$ following cutting the SWNTs in $HNO_3$ is consistent with an increase in the chemisorbed hydrogen population. The broadening and dramatic loss in intensity indicates that the nitric acid intercalation interferes with the resonance enhancement of the SWNT Raman modes. The process is reversible, however, as indicated by the return of intensity and appearance of the Raman modes at 1593 and 1567 $cm^{-1}$ upon heating to 1000 K. At this temperature a significant portion of the chemisorbed hydrogen resulting from the purification and cutting procedures has desorbed. The subsequent intensity loss and shift to higher frequency for the SWNT sample following exposure to $H_2$ at 500 torr again indicates charge transfer. These results therefore suggest that some of the 6.5wt% adsorbed $H_2$ undergoes an interaction with the SWNTs which is stronger than physisorption. Surprisingly the majority of the process is reversible as indicated by the regeneration of the Raman intensity upon degassing to 1000 K as displayed in Figure 9e. The fact that the curve displayed in Figure 9e is still slightly blue shifted may be attributed to a small population of hydrogen from the H2 exposure still remaining on the sample.

The exact location and nature of the SWNT $H_2$ adsorption sites is difficult to determine. However, collectively the results of this study give clues to the unique adsorption interactions. The shift to higher frequency and the decrease in Raman intensity following ultrasonication in $HNO_3$ is consistent with nitric acid intercalation resulting in charge transfer and a loss of SWNT resonance enhancement. The Raman data (Fig. 9d) also suggests a hydrogen SWNT interaction which disrupts the $sp^2$ pi character of the nanotubes indicating an interaction which is again stronger than physisorption. It is likely that this strong $H_2$ interaction with the SWNTs is the source of the high temperature TPD peak, and it is somewhat surprising that such a reaction is reversible. Since the low temperature hydrogen desorption peak evolves completely simply by sitting at room temperature overnight in vacuum, it most likely stems from a very weak interaction or physisorption.

While the present invention has been illustrated and described with reference to particular structures and methods of fabrication, it will be apparent that other changes and modifications can be made therein with the scope of the present invention as defined by the appended claims.

## Claims

1. A method of processing single-walled carbon nanotubes (SWNTs) for use in the formation of superbundles or hydrogen storage or both comprising the steps of:

(a) mixing a SWNT substrate in a solvent solution into a suspension; and

(b) agitating the suspension using an ultrasonic energy means.

2. The process of claim 1 wherein the solvent is a dilute acid or an oxidizing solution.

3. The process of claim 1 further comprising settling the suspension for a time sufficient to form an agglomeration of the bundles.

4. The process of claim 1 wherein the solvent is selected from a group consisting of deionized water, toluene, hexane, or alcohol.

5. The process of claim 1 wherein the solvent consists essentially of 50:50 methanol and water mixture.

6. The process of claim 1 wherein agitating comprises approximately 20 minutes at an ultrasonic power of about 90 Watts / $cm^2$.

7. The process of claim 1 wherein agitating further comprises applying ultrasonic energy to the suspension in a flowing state.

8. The process of claim 1 wherein agitating further comprises applying ultrasonic energy to the suspension in a static state.

9. The process of claim 1 wherein the substrate is a micro crystalline graphite.

10. The process of claim 1 wherein the substrate comprises greater than 98% SWNTs by weight.

11. The process of claim 1 wherein the substrate is an impure SWNT material.

12. The process of claim 1 wherein the substrate is a multi-walled carbon nanotube material.

13. The process of claim 2 wherein the dilute acid consists essentially of $HNO_3$.

14. The process of claim 2 further comprising degassing at an elevated temperature and absorbing hydrogen at an ambient temperature and pressure.

15. The process of claim 3 wherein the bundles range in size from 0.4 -1 microns in diameter and 5- 10 microns in length.

16. The process of claim 3 wherein the bundles comprise an essentially pure SWNTs, consisting essentially of, in percent by weight: SWNT's greater than 98 %; and metal less than 0.5 % wherein the SWNT's adsorb 2.0 to 7.0 % hydrogen.

17. The process of claim 13 wherein the dilute acid solution is about 5M $HNO_3$.

18. The process of claim 14 wherein agitation comprises 16 hours at 90 W / $cm^2$ and the degass proceeds at a temperature of about 825 K, the hydrogen adsorption comprising approximately 6.5 wt %.

19. The process of claim 14 wherein the hydrogen is adsorbed on at least two adsorption sites, the sites capable of desorption at about 370 and 630 K.

20. The process of claim 14 wherein ambient conditions comprise room temperature and 500 torr.

21. The process of claim 14 wherein agitation comprises a time in the range of 20 minutes - 24 hours using a sonication power in the range of 25 - 280 W/$cm^2$, the final absorption capacity of the bundles having a range of 2 - 7 wt %.

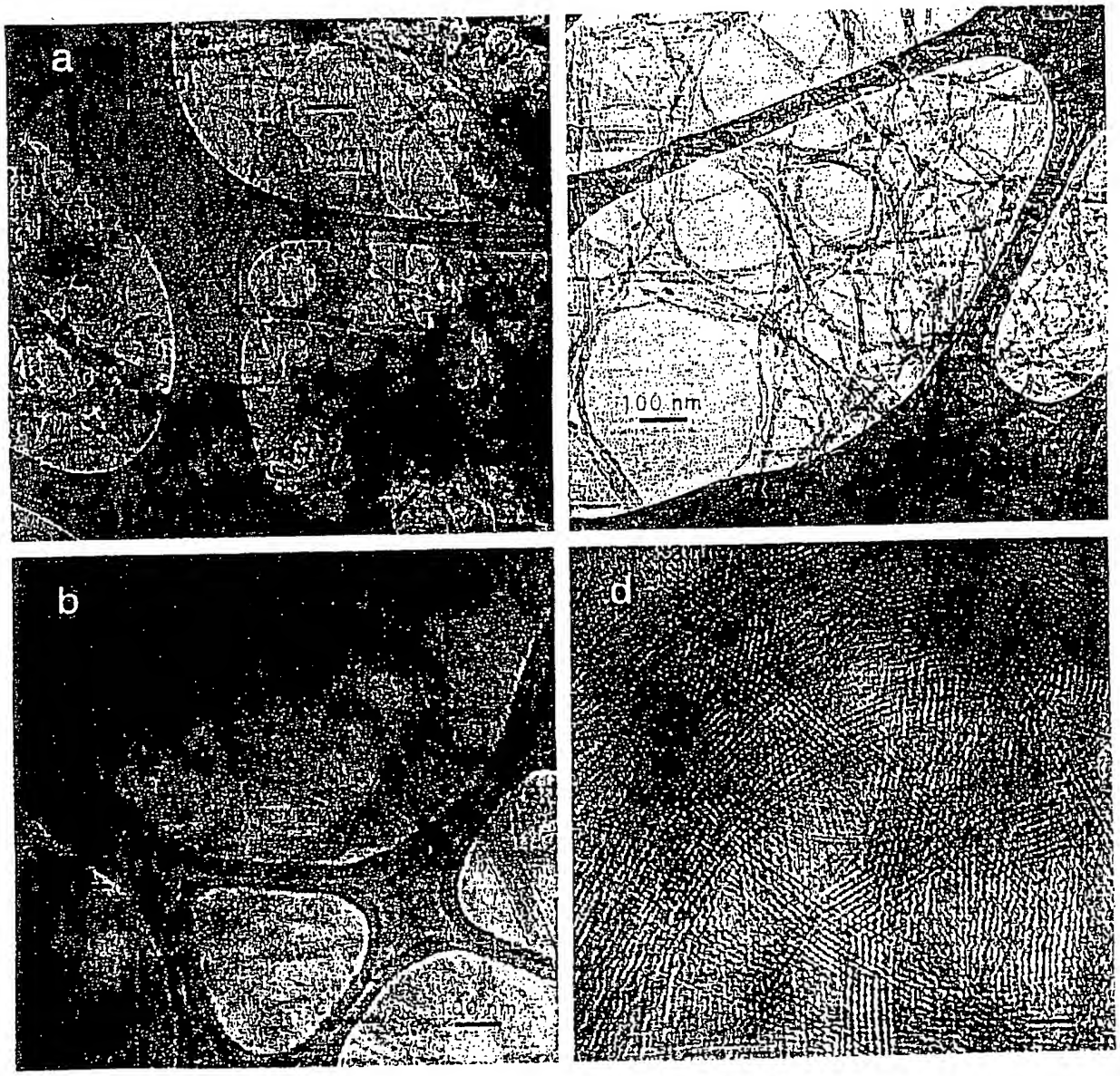


Figure 1

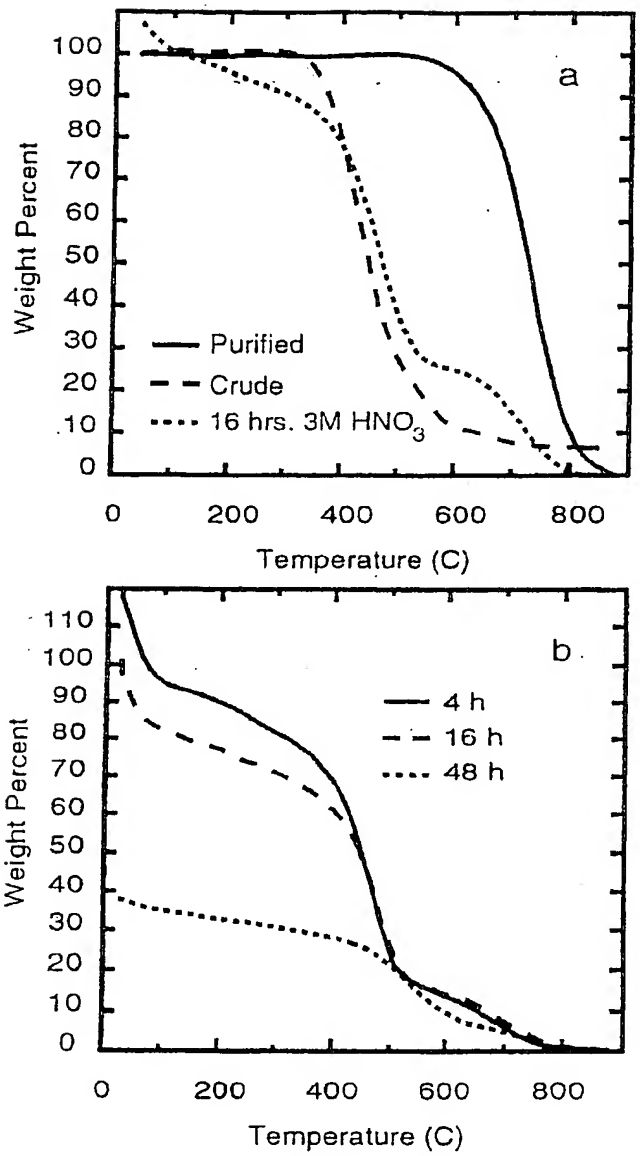
a
Weight Percent
100
90
80
70
60
50
40
30
20
10
0
Purified
Crude
16 hrs. 3M $HNO_3$
0
200
400
600
800
Temperature (C)
b
Weight Percent
110
100
90
80
70
60
50
40
30
20
10
0
4 h
16 h
48 h
0
200
400
600
800
Temperature (C)

**Figure 2**

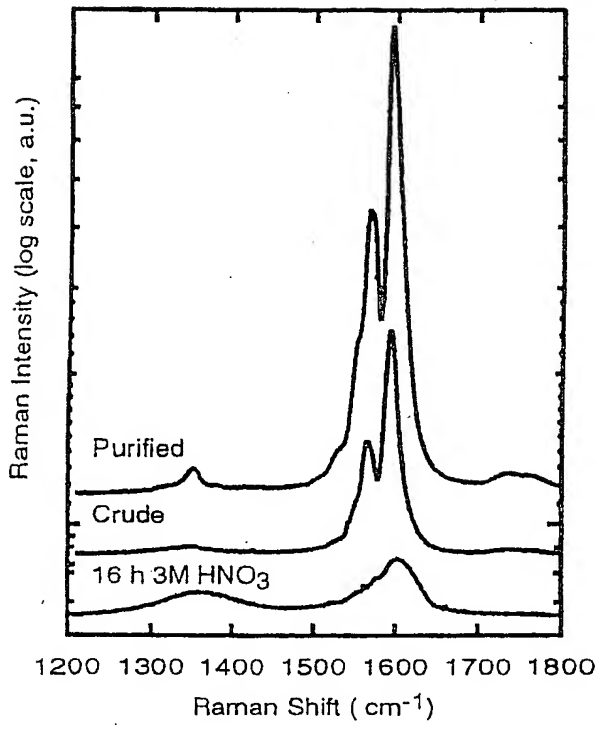
Raman Intensity (log scale, a.u.)
Purified
Crude
16 h 3M $HNO_3$
1200 1300 1400 1500 1600 1700 1800
Raman Shift ( $cm^{-1}$)

**Figure 3**

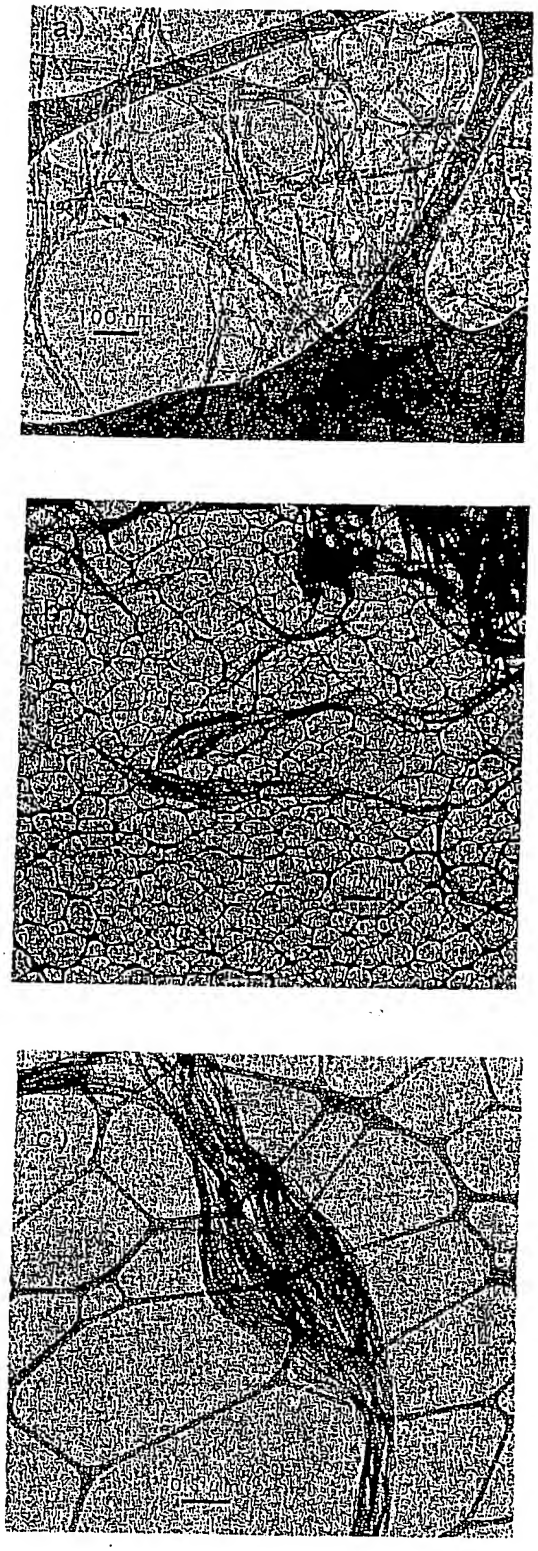


**Figure 4**

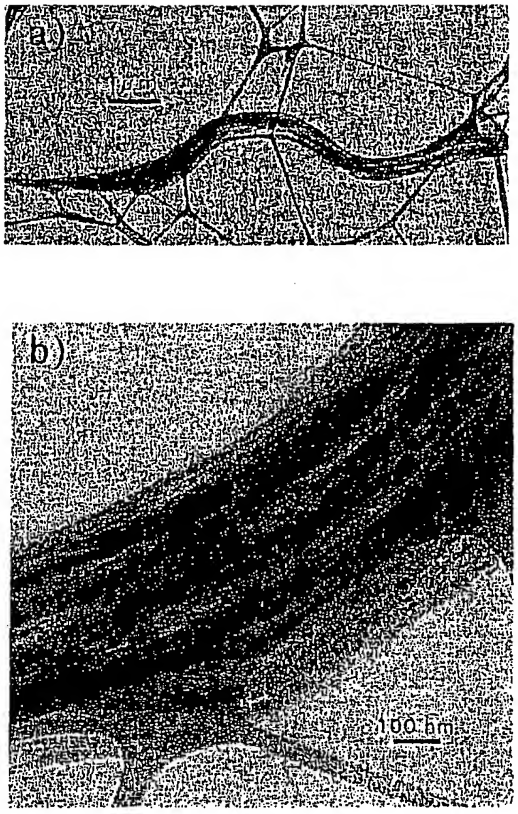


# Figure 5

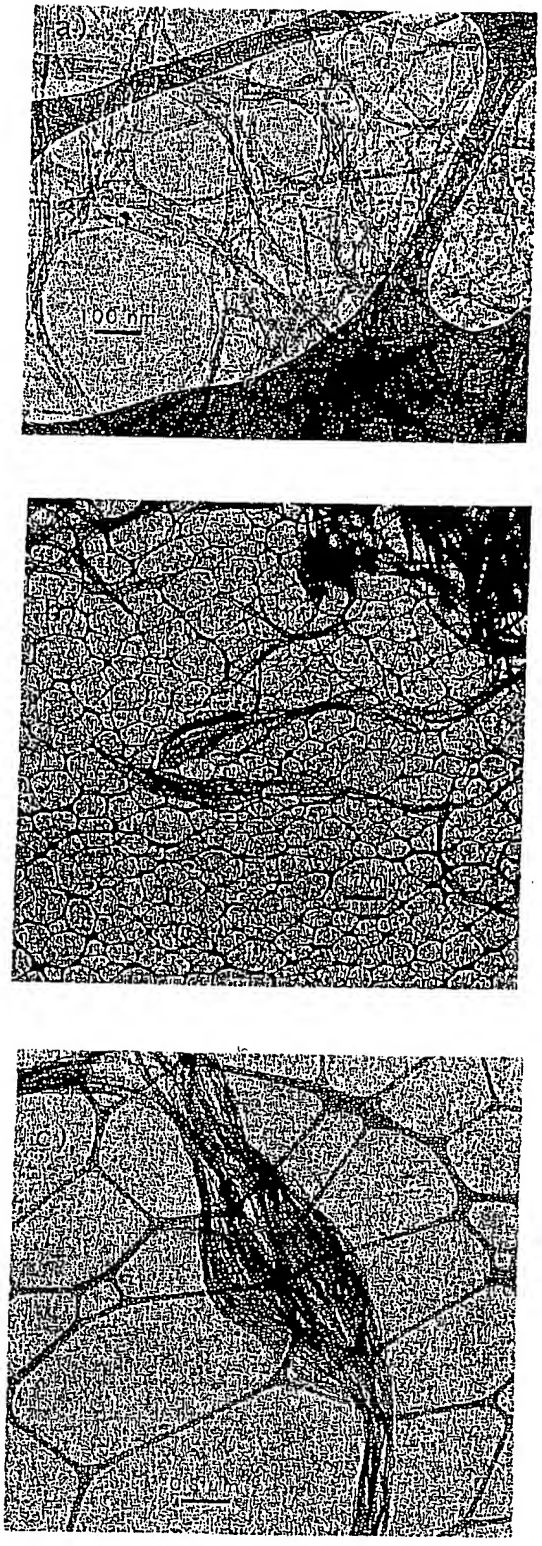


# Figure 4

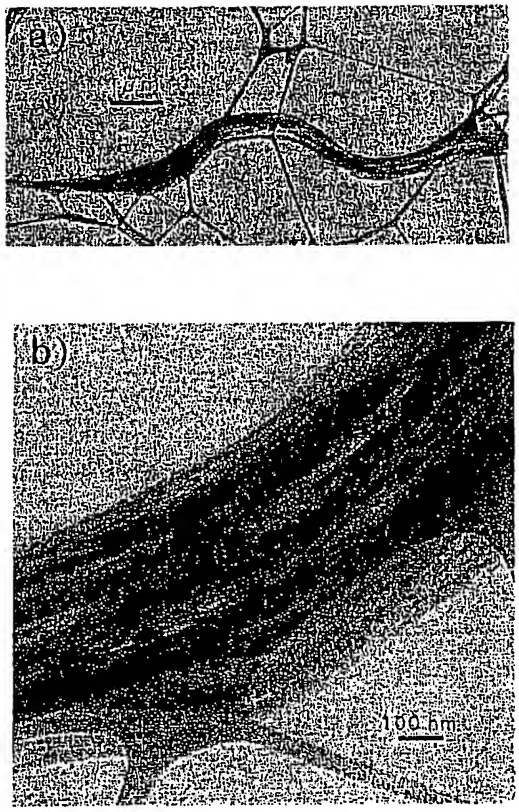


# Figure 5

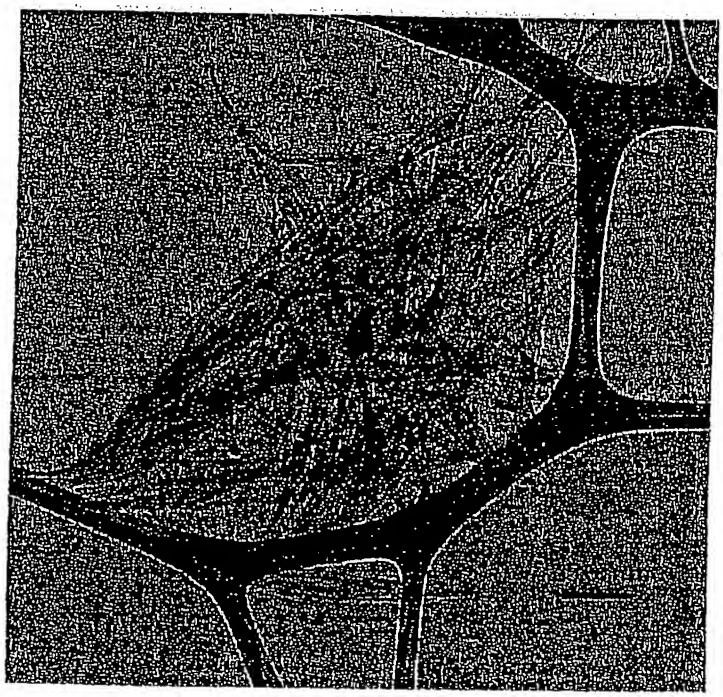

# Figure 6

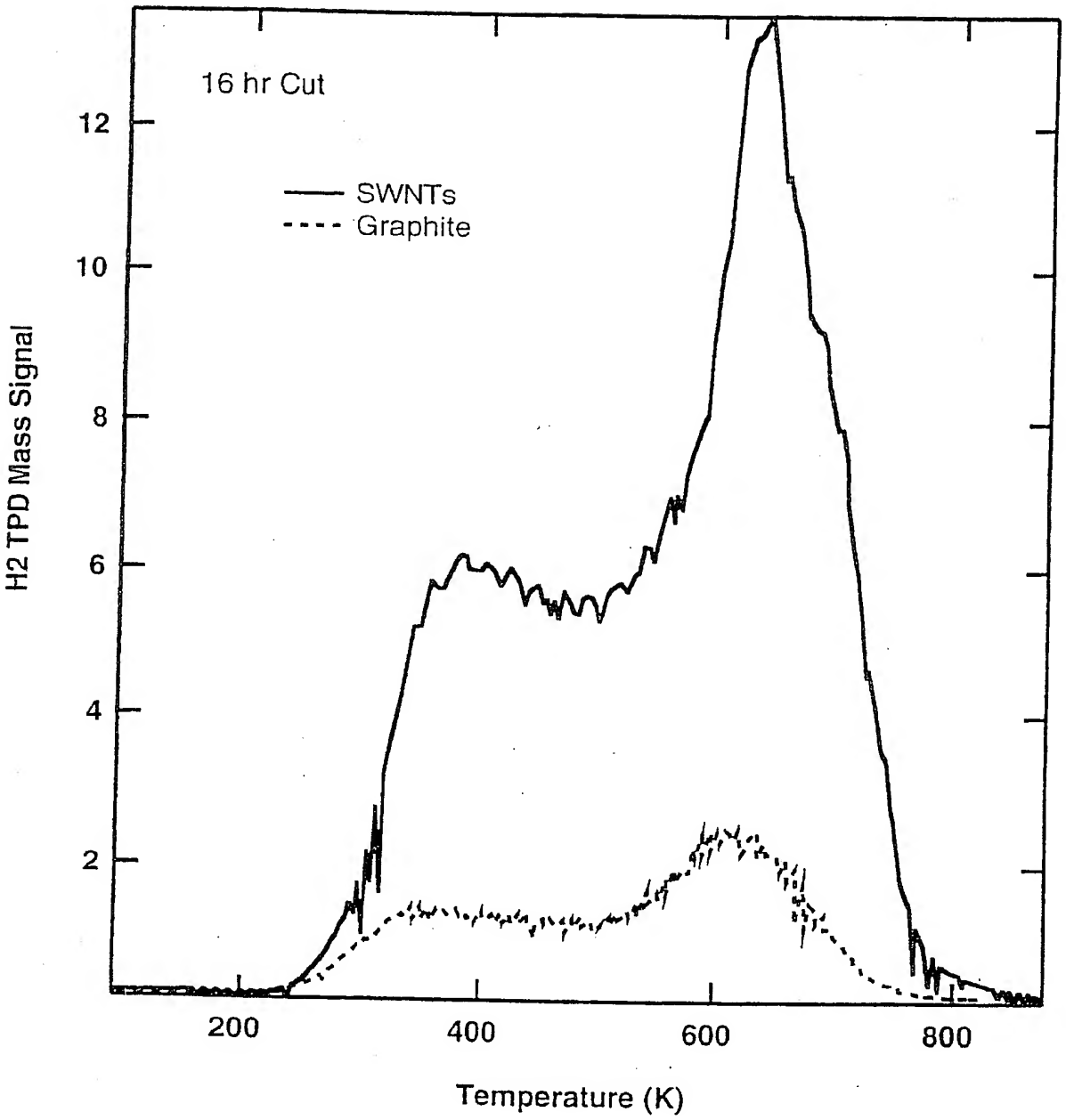
16 hr Cut
SWNTs
Graphite
H2 TPD Mass Signal
12
10
8
6
4
2
200
400
600
800
Temperature (K)

# Figure 7

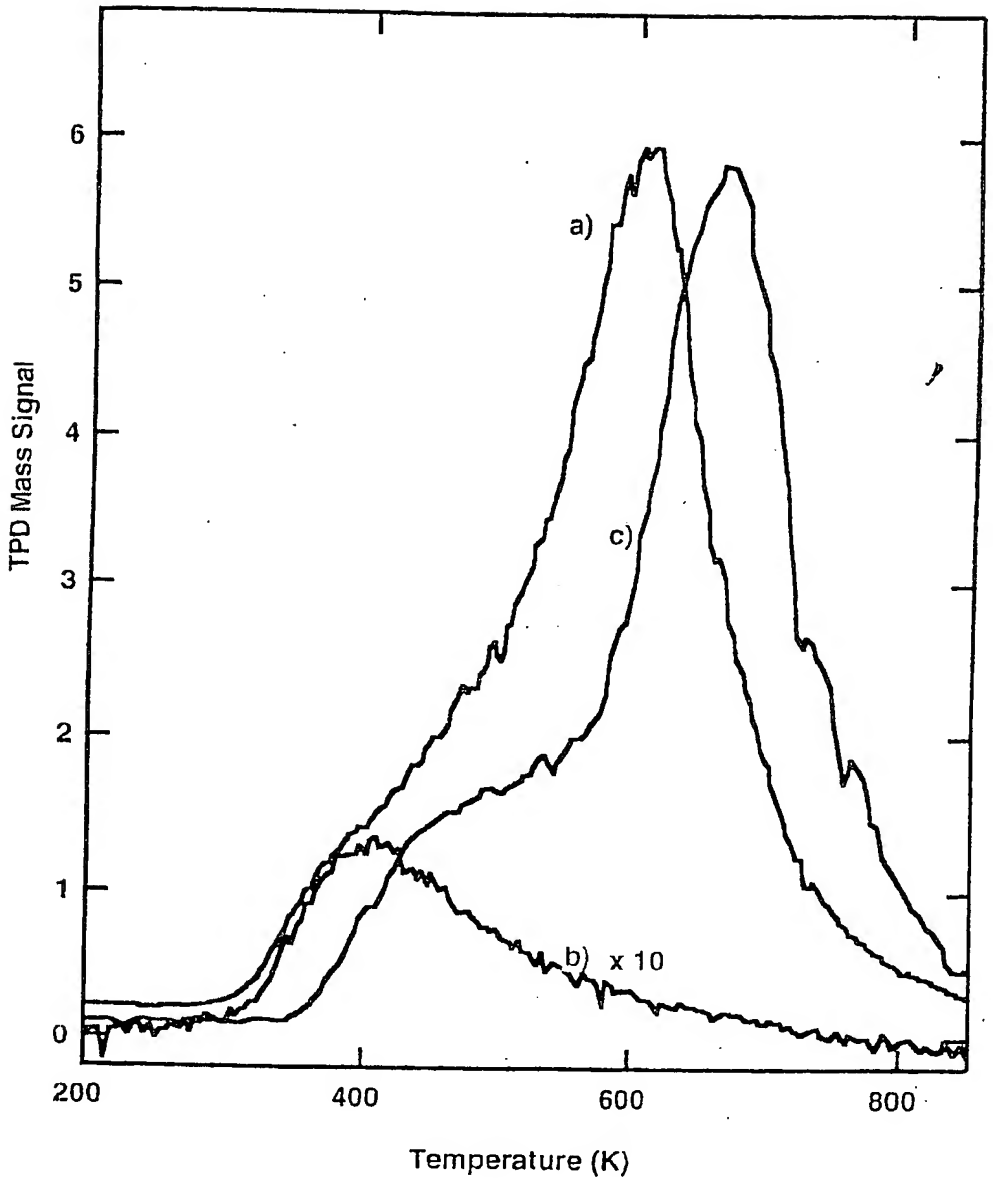
TPD Mass Signal
Temperature (K)
a)
b) x 10
c)
0
1
2
3
4
5
6
200
400
600
800

# Figure 8

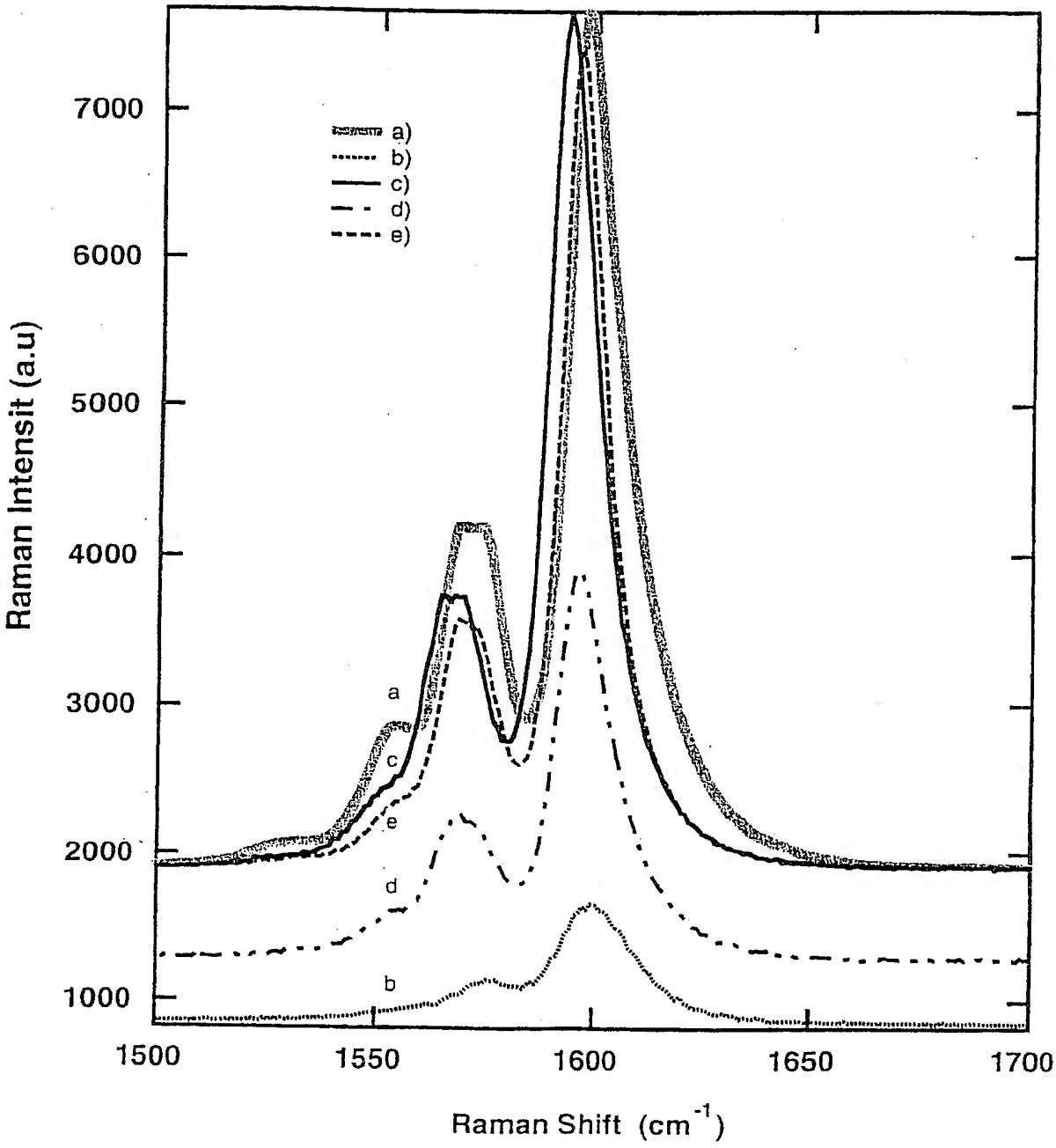
7000
6000
5000
4000
3000
2000
1000
Raman Intensit (a.u)
a)
b)
c)
d)
e)
a
c
e
d
b
1500
1550
1600
1650
1700
Raman Shift (cm-1)

**Figure 9**